PCCP

Accepted Manuscript

ROYAL SOCIETY OF CHEMISTRY

www.rsc.org/pccp

The Solid State Conversion Reaction of Epitaxial FeF_2(110) Thin Films with Lithium Studied by Angle-Resolved X-Ray Photoelectron Spectroscopy

Ryan Thorpe,* Sylvie Rangan, and Robert A. Bartynski†
Department of Physics and Astronomy and Laboratory for Surface Modification, Rutgers University, 136 Frelinghuysen Road, Piscataway, New Jersey 08854, United States

Ryan Whitcomb
Department of Applied Physics, University of Michigan, 450 Church Street, Ann Arbor, MI 48109, United States

Ali C. Basaran, Thomas Saerbeck,‡ and Ivan K. Schuller
Department of Physics and Center for Advanced Nanoscience, University of California San Diego, 9500 Gilman Drive, La Jolla, CA 92093, United States

The phase evolution and morphology of the solid state FeF_2 conversion reaction with Li has been characterized using angle-resolved x-ray photoelectron spectroscopy (ARXPS). An epitaxial FeF_2(110) film was grown on a MgF_2(110) single crystal substrate and exposed to atomic lithium in an ultra-high vacuum chamber. A series of ARXPS spectra was taken after each Li exposure to obtain depth resolved chemical state information. The Li-FeF_2 reaction initially proceeded in a layer-by-layer fashion to a depth of $\sim$ 1.2 nm. Beyond this depth, the reaction front became non-planar, and regions of unreacted FeF_2 were observed in the near-surface region. This reaction progression is consistent with molecular dynamics simulations. Additionally, the composition of the reacted layer was similar to that of electrochemically reacted FeF_2 electrodes. An intermediary compound $Fe_xLi_{2-2x}F_2$, attributed to iron substituted in the LiF lattice, has been identified using XPS. These measurements provide insight into the atomistics and phase evolution of high purity FeF_2 conversion electrodes without contamination from electrolytes and binders, and the results partially explain the capacity losses observed in cycled FeF_2 electrodes.

I. INTRODUCTION

Iron (II) fluoride-based nanocomposites are promising candidates as active materials in lithium ion conversion battery cathodes. Upon exposure to lithium ions in an electrochemical cell, FeF_2 is believed to undergo the following reversible reaction:[1–4]

$$2Li^+ + 2e^- + Fe^{(2+)}F_2 \rightarrow 2LiF + Fe^{(0)}. \qquad (1)$$

Although FeF_2 is a bulk insulator with a band gap of about 2 eV,[5] the use of FeF_2 nanoparticles embedded in a chemically inert conducting carbon matrix has been shown to increase the conductivity of FeF_2-based electrodes sufficiently to allow for efficient charge transport.[1,2] Additionally, the volumetric expansion of FeF_2 upon lithiation is only 16%, which is small enough to avoid strain-induced damage to the cell during cycling.[1] FeF_2 has a theoretical specific capacity of 571 mAh/g, while working devices have exhibited capacities as high as 350-450 mAh/g for several cycles.[3,6] These values represent a significant improvement over the theoretical and practical capacities of modern $LiCoO_2$ electrodes, which are 272 mAh/g and 145 mAh/g respectively.[7]

This increase in charge storage is due to a fundamental difference in the reaction mechanism of iron fluoride particles. Conventional Li-ion intercalation batteries rely on the insertion/deinsertion of Li^+ ions into planar or columnar channels in a cathode material such as $LiCoO_2$.[8] In practice, only $\sim$ 0.5 Li ions per formula unit can be inserted and removed from the cathode without significantly altering the crystalline structure of the $LiCoO_2$ and destroying the structural integrity of the cathode. Conversely, the Li-FeF_2 conversion involves extensive morphological and structural transformations as FeF_2 is converted to metallic Fe and LiF. This reaction transfers two Li ions, and hence two electrons, per formula unit.[4,5,9,10]

Despite the apparent advantages of using FeF_2 cathodes, their implementation has thus far been limited by capacity fading and high voltage hysteresis upon cycling. These issues have been attributed in part to limited lithium mobility within the FeF_2/Fe/LiF composite and to a loss of active material from parasitic reactions.[4,10] Recent molecular dynamic (MD) simulations by Ma and Garofalini[11,12] have suggested that the FeF_2(110) and (001) crystalline faces react differently upon exposure to lithium. The FeF_2(001) orientation exposes [001] channels in which the kinetic barrier for Li ion diffusion is less than 0.05 eV. These channels facilitate lithium diffusion into the bulk of the FeF_2, which allows the conversion reaction to proceed rapidly from the surface to the bulk of the material. Conversely, the FeF_2(110) surface has a high ($\sim$ 1 eV) kinetic barrier for Li transport into the bulk, which causes the conversion reaction to initiate in a layer-by-layer fashion. However, as the reaction proceeds several layers into the FeF_2 surface, grain boundaries between Fe nanoparticles and LiF provide pathways for lithium diffusion into the crystal. These interfacial regions then become preferential nucleation points for the

sub-surface conversion reaction, causing a non-planar reaction front as the conversion reaction proceeds into the $FeF_2(110)$ crystal.

In order to bridge the gap between these MD simulations and bulk measurements of electrochemically cycled FeF_2 electrodes, it is necessary to study high-purity FeF_2 samples in the absence of electrolytes, binders, and separators which affect cell performance. To this end, high-purity epitaxial $FeF_2(110)$ thin films were grown and exposed to atomic lithium in an ultra-high vacuum chamber. The (110) orientation has the lowest surface energy of the FeF_2 crystalline faces, so this surface is expected to dominate the nanocrystalline FeF_2 composites used in electrochemical cells.[12] The resulting solid state reaction was then characterized by angle-resolved x-ray photoelectron spectroscopy (ARXPS) in order to produce a nanometer-scale model of the reaction progression. The results obtained from these ARXPS measurements indicate that the reaction front initially progresses in a layer-by-layer fashion, forming a planar interface between the reacted overlayer and the unreacted FeF_2 substrate. This is consistent with MD simulations for small lithium exposures.[11] However, when the reacted layer reached a depth of $\sim 1.2\,\text{nm}$ into the film, the reaction front deviated from this planar geometry and the reacted overlayer acquired a non-uniform thickness. This behavior is consistent with a model in which preferential reaction nucleation occurs in the sub-surface regions of the $FeF_2(110)$ crystal. The chemical composition of the reaction products and the phase evolution of the FeF_2 film agree with the results of pair distribution function (PDF), galvanostatic intermittent titration technique (GITT), and XPS studies of cycled FeF_2 electrodes, which found evidence of the formation of an intermediate compound identified as $Fe_xLi_{2-2x}F_2$.[4,6]

II. EXPERIMENTAL METHODS

A. Sample Preparation

Epitaxial $FeF_2(110)$ films were grown on $MgF_2(110)$ single crystal substrates by electron beam evaporation of FeF_2 powder (Cerac Inc.) at a rate of 0.05 nm/s. The temperature of the MgF_2 substrates was maintained at 300°C to enhance the crystallinity of the film. During deposition, the chamber pressure was less than $2 \times 10^{-7}\,\text{Torr}$. The FeF_2 structure and crystallinity were investigated using x-ray reflectometry (XRR), x-ray diffraction (XRD), and helium ion microscopy (HIM). The x-ray data was acquired using a D8 Discover Bruker rotating anode diffractometer with Cu Kα ($\lambda = 1.54$Å) radiation. The film was exposed to air during the transfer from the growth chamber to the ultra-high vacuum analysis chamber. In order to remove adsorbates from the surface, the FeF_2 film was degassed at 300°C in ultra-high vacuum (UHV) for 30 minutes. This temperature was sufficiently high to remove most surface impurities without reducing the FeF_2 film.

Atomic lithium was deposited onto the surface of the FeF_2 film at room temperature using a lithium getter source (SAES Getters). The lithium source was well degassed prior to exposure, and the pressure in the vacuum chamber was kept below $5 \times 10^{-9}\,\text{Torr}$ during lithiation. The Li exposure rate was estimated to be 0.07 nm/min, which was chosen to be slow enough to prevent the accumulation of metallic Li at the surface of the FeF_2 film.

B. Angle-Resolved XPS

X-ray photoelectron spectroscopy measurements were performed using a Thermo Scientific ESCALAB 250Xi using a monochromated Al Kα x-ray source with an energy of 1486.6 eV. The total resolution of the instrument was 0.5 eV. To obtain angular resolution, the half-angle of acceptance of the electron analyzer was set to 10° and the sample was rotated with respect to both the x-ray source and detector from 0° to 50° in 5° increments. In this work, the emission angle is measured with respect to the surface normal.

In order to minimize the buildup of electrical charge during XPS measurements, charge compensation was performed using a dual beam flood source of low-energy Ar^+ ions and 1 eV electrons. Spectra taken before and after these measurements showed no x-ray or ion induced damage. A small amount of peak broadening attributed to differential charging was observed after prolonged lithium exposures, likely due to the inhomogeneity in the conductivity of the conversion reaction products. The C 1s spectral component at -284.8 eV arising from adventitious carbon was chosen as a binding energy reference.[13] XPS spectra were analyzed by subtracting Shirley backgrounds and fitting the remaining core level features with Voigt profile components,[14] or, in the case of Fe 2p spectra, with broadened reference spectra taken from pure FeF_2 and Fe metal samples.

Angle-resolved XPS (ARXPS) makes use of the nanometer-scale inelastic mean free path (IMFP) of electrons in solid media to obtain depth resolved chemical and elemental information from samples whose surface roughness is less than 1-2 nm. For a thin ($< 5\,\text{nm}$) overlayer of material A (thickness d) on a substrate B, the ratio R of XPS intensities from species A and B is well approximated by

$$R(\theta, d) = \frac{I_\text{A}}{I_\text{B}} = \frac{I_\text{A}^\infty}{I_\text{B}^\infty}\left[\frac{1 - \exp\left(-d/\lambda_\text{AA}\cos\theta\right)}{\exp\left(-d/\lambda_\text{BA}\cos\theta\right)}\right] \qquad (2)$$

where λ_{ij} is the IMFP in material j for electrons emitted from material i, θ is the electron emission angle measured with respect to the surface normal, and I_k^∞ is the XPS intensity of an infinitely thick layer of material k.[15] To increase the precision of the ARXPS analysis, an effective attenuation length (EAL) was substituted for each IMFP in Equation 2 in order to account for elastic scattering of photoelectrons at large emission angles.[16–18] EALs were

calculated as a function of emission angle and overlayer thickness for each compound using the NIST Electron EAL Database.[19] Equation 2 can be simplified by assuming that the EAL is constant:

$$R(\theta, d) \approx R^{\infty}\left[\exp\left(\frac{d}{\lambda \cos\theta}\right) - 1\right] \quad (3)$$

where $R^{\infty} = I_{\mathrm{A}}^{\infty}/I_{\mathrm{B}}^{\infty}$. This expression is then linearized by rearranging terms and taking the natural logarithm:

$$\ln\left(1 + R/R^{\infty}\right) \approx d/\lambda \cos\theta. \quad (4)$$

To calculate the thickness and uniformity of the reacted layers as precisely as possible, Equation 2 was used. Since this equation has no analytical solution for d, a multi-layer model of the Li-FeF_2 reaction was constructed and used to predict the variation of R as a function of θ. The details of this model will be explained further in the subsequent section. Data will be analyzed using Equation 4 so that it can be presented in a linearized form.

III. RESULTS AND DISCUSSION

A. Characterization of the FeF_2(110) Film

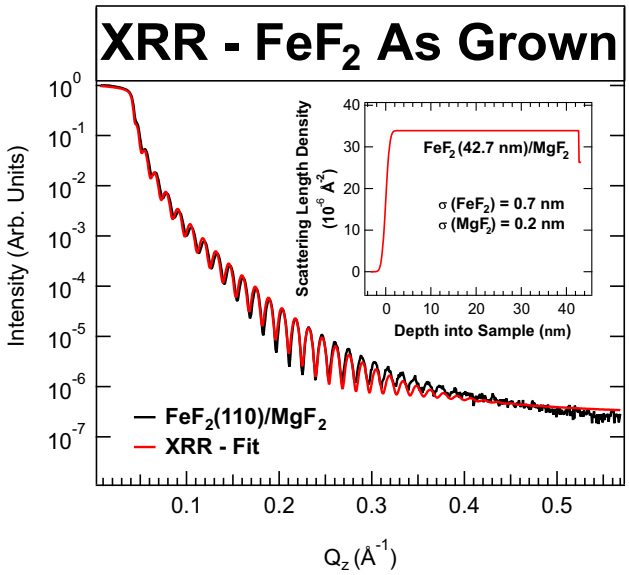

FIG. 1: X-ray reflectometry data from the as-grown FeF_2(110) film indicating a film thickness of 42.7 nm and a surface roughness of $\sigma = 0.7$ nm.

Figure 1 shows x-ray reflectometry (XRR) data from the as-grown FeF_2(110) thin film. The fit to the XRR data was performed with MOTOFIT software by assuming a slab model density profile (Figure 1: inset).[20] The film thickness was assumed to have a Gaussian distribution with a standard deviation σ. These measurements indicate an FeF_2 film thickness of 42.7 nm and a surface roughness of $\sigma = 0.7$ nm. Additionally, helium ion microscopy images of the film indicated that the lateral dimensions of the FeF_2 domains were 10-15 nm.

After transferring the FeF_2(110) film to the XPS chamber and annealing at 300°C to remove surface contamination, a series of normal emission XPS spectra was taken to measure the purity and stoichiometry of the film. These spectra are shown in Figure 2. The Fe 2p core level spectrum (inset (a)) is composed of broad $2p_{3/2}$ and $2p_{1/2}$ states at binding energies of -711 eV and -725 eV and small satellite features whose centroids are at ~ 6 eV higher binding energy than the main doublet peaks. The F 1s core level spectrum (inset (b)) is composed of a single feature at -685 eV. These Fe 2p and F 1s features are consistent with previous studies of high purity FeF_2 thin films and powders.[5,21] Normalizing the F 1s and Fe 2p intensities by their respective Scofield factors and detector functions yielded a F:Fe ratio of (1.8 ± 0.1):1, confirming the stoichiometry of the film. The O 1s core level spectrum (inset (c)) is composed of three peaks. The main peak at a binding energy of -530 eV is attributed to FeO, which formed due to the oxidation of the FeF_2 film in air.[22] The F:O ratio suggests that only the topmost layer of FeF_2 was oxidized. The smaller O 1s peaks at -531.5 and -532 eV are attributed to hydroxyl and water contamination on the surface of the sample.[23,24] These intensities are consistent with one monolayer of surface contamination. The C 1s spectrum (inset (d)) exhibits a large component at -284.8 eV and two smaller components at -287.5 and -289.0 eV. These are indicative of adventitious carbon contamination, and their total intensity is consistent with slightly less than one monolayer of contamination on the surface of the film.[13] Despite the surface contamination present on the FeF_2 film, the formation of lithium oxides, hydroxides, and carbonates was not observed upon exposure to lithium. Indeed, the O 1s and C 1s spectra were unchanged after the lithium depositions, and hence these contaminants were not believed to significantly affect the Li-FeF_2 reaction. It should be noted in subsequent sections that, due to its energy overlap with the Fe 3p core level, the Li 1s peak was not evaluated in this work.

B. Chemical State Analysis

The FeF_2(110) film was exposed to Li in intervals ranging from 5 to 20 minutes at a rate of about 0.07 nm/min, for a total lithiation time of 160 minutes. After each lithiation, a series of XPS spectra was acquired. In order to extract quantitative chemical information from the XPS data, a least squares fit was performed for each Fe 2p spectrum using a linear combination of reference spectra taken from pure Fe metal and FeF_2 samples (Alfa Aesar). Figure 3 shows a normal emission Fe 2p XPS spectrum after 35 minutes of total Li exposure. The XPS data, shown as black dots, exhibits multiple peaks corre-

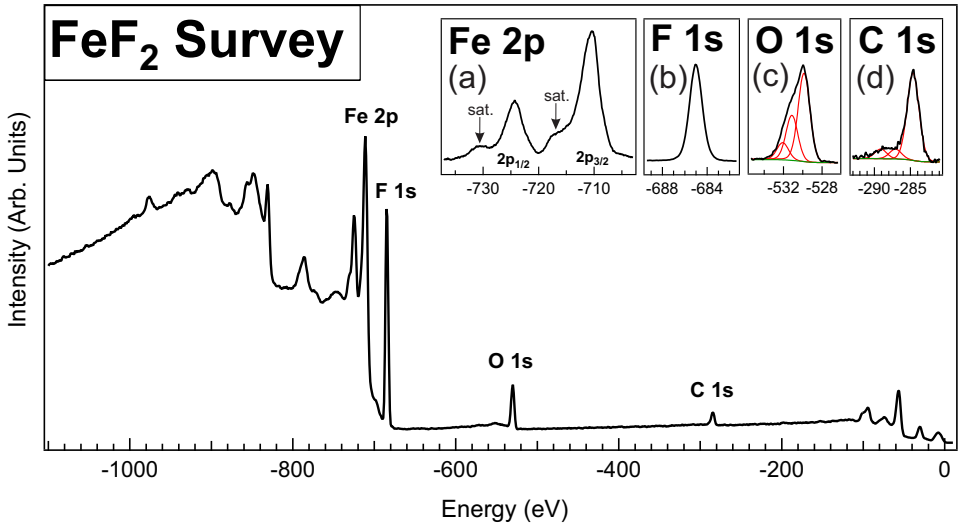

FIG. 2: XPS Survey spectrum of an $FeF_2(110)$ film after degassing at 300°C in UHV. Inset, core level spectra indicate the presence of small amounts of hydroxyl and carbon containing species at the surface and the formation of FeO in the topmost layer of the film.

sponding to different chemical states of iron. The Fe^{2+} (FeF_2, red) and Fe metal (Fe^0 gray) reference spectra were not sufficient to fit the data, suggesting the formation of an intermediate compound during the conversion reaction. To account for this missing intensity, an additional spectral component was constructed from the final (160 minute) lithiation spectrum by subtracting Fe metal and FeF_2 components from the Fe 2p data. The details of this procedure are presented in Section SII of the Supplemental Material. The resulting lineshape, shown in yellow in Figure 3, exhibited 2p doublet peaks at binding energies of -709 eV and -723 eV and intense satellite features at -716 eV and -730 eV.

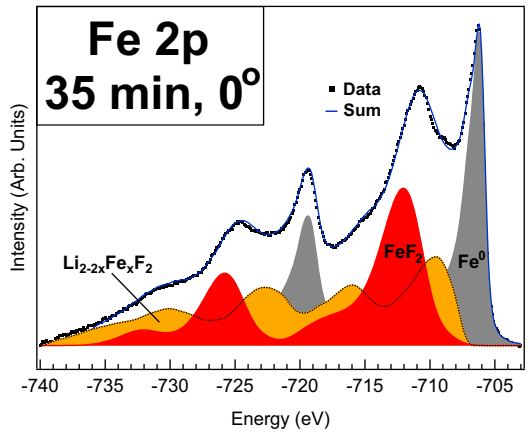

FIG. 3: XPS spectrum of the Fe 2p core level at normal emission after the $FeF_2(110)$ film underwent 35 minutes of total Li exposure. The data is shown as black dots, and the sum of the spectral components is a solid blue line. Iron metal and iron fluoride reference spectra were obtained from high-purity samples (Alfa). Three components are needed to fit this and all other Fe 2p spectra upon lithiation, suggesting the presence of a ternary Li-Fe-F compound.

The peak positions and lineshape of this chemical species are not consistent with any known iron fluoride, oxide, or oxyfluoride compounds.[5,21,25,26] However, several recent studies provide insight into the possible nature of this compound. First, recent pair distribution function (PDF) studies of electrochemically cycled FeF_2 by Ko and coworkers[4] observed an expansion of the LiF rocksalt lattice upon delithiation. This was attributed to the incorporation of iron in the LiF lattice to form $Fe_xLi_{2-2x}F_2$, with x estimated to be between 0.4 and 0.5. Additionally, MD simulations by Ma and Garofalini predicted the formation of a ternary Fe-Li-F compound upon the lithiation of both $FeF_2(110)$ single crystals and FeF_2 nanoparticles.[11,12] Consequently, the additional Fe 2p component observed in the lithiated FeF_2 spectrum is attributed to the ternary compound $Fe_xLi_{2-2x}F_2$.

The $Fe_xLi_{2-2x}F_2$ spectral component was necessary to fit every Fe 2p spectrum acquired after the initial lithiation, and its integrated intensity was found to be between 85% and 110% that of the Fe^0 component for every Li exposure, which is consistent with $x \approx 0.5$. This chemical species was also identified in XPS spectra of electrochemically cycled FeF_2 electrodes.[6] Using $x \approx 0.5$, this compound can be written as $Fe_{0.5}LiF_2$, and hence an alternative FeF_2 conversion reaction pathway can be described by

$$\mathrm{Li} + \mathrm{FeF_2} \rightarrow \mathrm{Fe_{0.5}LiF_2} + 0.5\mathrm{Fe}. \quad (5)$$

In the following sections, it will be assumed that $x = 0.5$, and this chemical compound will be referred to as $Fe_{0.5}LiF_2$. Since the amount of $Fe_{0.5}LiF_2$ was observed to increase monotonically with each Li exposure, this compound is believed to be a stable product of the FeF_2 conversion reaction.

C. ARXPS of the Li-FeF_2 Reaction

XPS was used to determine the changes in FeF_2 film stoichiometry after each lithium exposure. Figure 4(a) shows the normal emission Fe 2p spectra acquired after each lithium exposure. The spectra have been normalized to their maximum intensities to allow for a visual comparison. The bottom spectrum in Figure 4(a) is the same as the Fe 2p spectrum shown in Figure 2. Upon exposure to lithium, new features appeared at binding energies of -707 eV and -720 eV, attributed to the $2p_{3/2}$ and $2p_{1/2}$ electronic states of iron metal.[5] The intensity of these features increased monotonically as a function of Li exposure while the FeF_2 intensity decreased simultaneously, in accordance with the conversion reaction proposed in Equation 5. The topmost Fe 2p spectrum, acquired after 160 minutes of total Li exposure, mainly exhibits Fe^0 and $Fe_{0.5}LiF_2$ features with FeF_2 accounting for only 12% of the spectral intensity.

In order to obtain depth-resolved information from the lithiated FeF_2 film, a series of angle-resolved XPS spectra was taken at 5° increments after each lithiation. Figure 4(b) shows one such series acquired after 35 minutes of total Li exposure and the three Fe 2p components required to fit each spectrum. These spectra are representative of the ARXPS data acquired after each lithiation step and are presented as an example. The heights of the spectra have been normalized to the intensity of the Fe^0 features in order to enhance their visual differences. At normal emission (0°), the Fe 2p spectrum exhibits features from FeF_2, Fe^0, and $Fe_{0.5}LiF_2$ chemical states. As the electron emission angle increases, the integrated intensity of the FeF_2 component decreases relative to the Fe^0 component. Conversely, the $Fe_{0.5}LiF_2$ component maintains a 1:1 ratio with the Fe^0 component for all angles. This suggests that the Fe^0 and $Fe_{0.5}LiF_2$ species formed an overlayer atop the FeF_2 film. Since no angular variation in the Fe^0:$Fe_{0.5}LiF_2$ ratio was observed for any Li exposure, only the Fe^0:FeF_2 ratio was necessary to calculate the thickness and uniformity of the reacted $Fe_{0.5}LiF_2$+Fe^0 overlayer. Hence, the Fe^0:FeF_2 ratio (R) was analyzed after each lithium exposure. Figure 5 shows the evolution of R the as a function of emission angle after 5 minutes (a) and 35 minutes (b) of total lithium exposure. The solid and dashed lines represent fits to these data based on a model described below.

For both 5 minute and 35 minute Li exposures, the value of R (shown as black dots in Figure 5) increases as a function of θ, again consistent with an overlayer of Fe and $Fe_{0.5}LiF_2$ on the FeF_2 substrate. The error bars shown were calculated from the residuals of the Fe 2p fit and do not account for the uncertainty caused by variations in the position/shape of the x-ray beam spot as the sample was tilted. For the 5 minute exposure, shown in Figure 5(a), the fit to the data (solid red line) was obtained from Equation 2 by considering a uniformly thick reacted overlayer consisting of stoichiometric amounts of Fe and $Fe_{0.5}LiF_2$.

The ARXPS model assumed that the number of photoelectrons passing through each species was proportional to the specific volume of that species. This is mathematically equivalent to dividing the overlayer vertically into discrete regions of $Fe_{0.5}LiF_2$ and Fe, as illustrated in Figure 6(a). For small overlayer thicknesses ($d < 5$ nm), this approximation should be accurate since the typical dimensions of the Fe nanoparticles are expected to be between 2-5 nm.[5,11,12] Consequently, the particles should extend from the sample surface to the reaction interface, as shown in Figure 6(b). Hence, the agreement between the data and the uniformly thick overlayer model ($r^2 = 0.958$) suggests that the conversion reaction front was planar for 5 minutes of lithium exposure. The reacted overlayer thickness is estimated to be 0.5 ± 0.1 nm, which is consistent with the conversion of about one bilayer of FeF_2. The reaction front remains uniform for overlayer thicknesses up to 1.2 ± 0.1 nm. More information about the ARXPS model for this and subsequent lithium exposures is presented in Section SIV of the Supplemental Material.

Figure 5(b) shows the $R(\theta, d)$ curve (black data points) obtained after 35 minutes of total Li exposure, and two fits based on Equation 2 assuming a uniformly thick reacted overlayer (solid red line) and a reacted overlayer with non-uniform thickness (dashed red line). The model with a non-uniform overlayer thickness agrees well with the data ($r^2 = 0.978$) and is described in more detail below. For this and subsequent Li exposures, the reaction model was modified to account for a non-planar interface between reacted and unreacted materials, as shown in Figure 6(c). The best agreement between the measured and predicted $R(\theta, d)$ curves was obtained for models in which (87 ± 2)% of the reaction front area proceeded to a depth of $D = 3.8 \pm 0.3$ nm, while the remaining (13 ± 2)% remained at a depth of $d = 1.2 \pm 0.1$ nm, as shown in the idealized and realistic models in Figure 6(a) and (b) respectively. In other words, (13 ± 2)% of the near-surface FeF_2 remained unreacted after the reaction front proceeded beyond 1.2 nm into the film. Again, this variation in the reacted overlayer thickness is consistent with MD simulations.[11]

Figure 7 shows the linearized $R(\theta, d)$ plots, which were constructed from the approximation shown in Equation 4. By plotting $\ln(1 + R/R^\infty)$ vs. $\sec\theta$, the curves that correspond to uniform reacted overlayers should appear as straight lines whose slopes are proportional to the overlayer thickness and whose (artificially extrapolated) y-intercepts are at the origin.

Using this simple method of analysis provides an intuitive explanation of the relationship between the $R(\theta, d)$ curves and the diagrams in Figure 6. The values of d, D, and the percentage of unreacted FeF_2 covered by a thin overlayer are summarized in Table I. For small Li exposures (overlayer thicknesses less than ~ 1.2 nm), the reaction front proceeds uniformly through the film. Consequently, the data corresponding to 5 minutes (0.5 nm) and 15 minutes (1.2 nm) of total Li exposure are well-fit

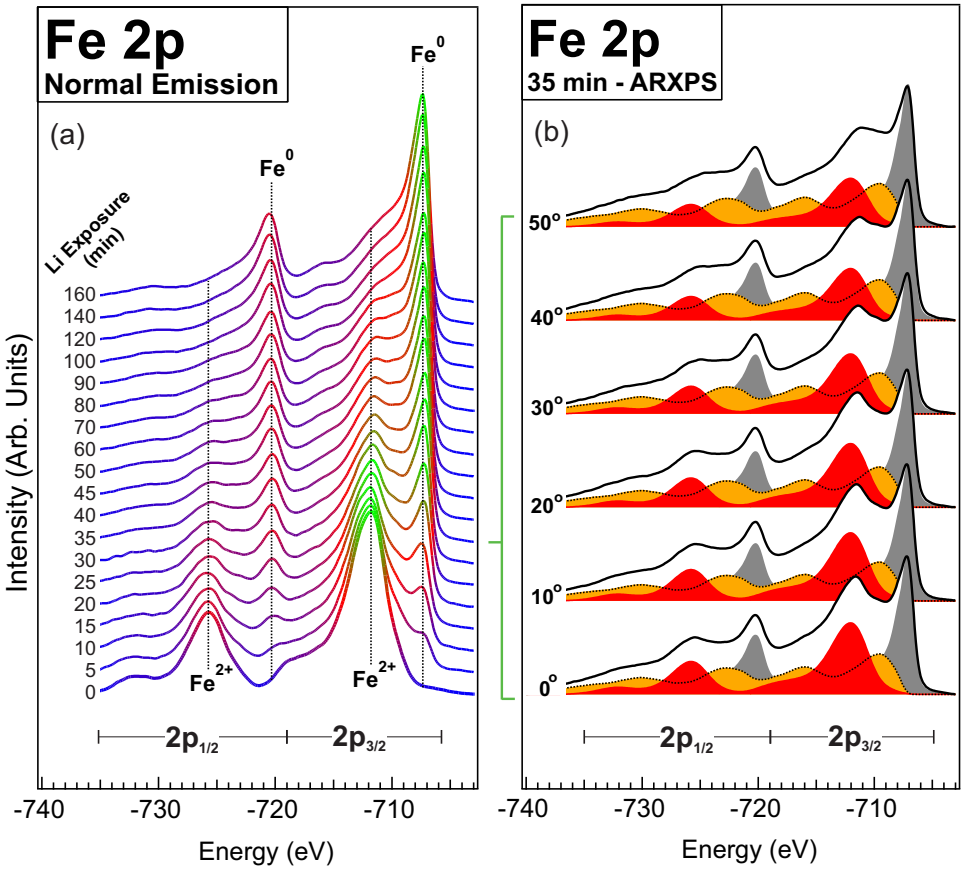

FIG. 4: (a) Evolution of the normal emission Fe 2p XPS spectra from $FeF_2(110)$ before and after sequential Li exposures. (b) Angular dependence of the Fe 2p spectrum after 35 minutes of total Li exposure. The spectra have been normalized by height in order to accentuate the differences between their lineshapes.

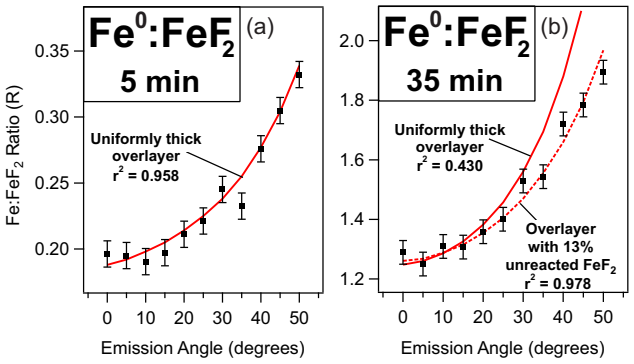

FIG. 5: The Fe^0:FeF_2 ratio (R) versus electron emission angle after 5 minutes (a) and 35 minutes (b) of total lithium exposure. The solid (dashed) curves are fits based on models with reacted overlayers of uniform (variable) thickness.

by $R(\theta, d)$ curves derived from uniformly thick overlayer models (shown as solid red lines). For greater overlayer thicknesses, the reaction front becomes non-planar, and hence the curves corresponding to > 25 minutes (2.5 nm and thicker) are not well fit by uniformly thick overlayer models, but instead by models with non-uniform overlayers (dashed red lines). When the reaction front proceeds deeper than the escape depth of the Fe 2p photoelectrons ($D > 10$ nm), the film appears as a mixture of Fe, $Fe_{0.5}LiF_2$, and unreacted FeF_2. At these large lithium exposures, the XPS data no longer varies with emission angle, and hence no information can be garnered about the depth of the reaction front. However, the amount of unreacted FeF_2 is observed to slowly decrease from $(13 \pm 2)\%$ to $(8 \pm 1)\%$, as seen by the increase in the Fe:FeF_2 ratio between the > 12 nm and > 20 nm curves in Figure 7. For these $R(\theta, d)$ curves, the low intensity of the FeF_2 component in the Fe 2p spectra causes a large uncertainty in the value of R. However, the position and shape of the x-ray beam on the sample also contributed to the error, which likely caused the R values for the 0° data points to differ significantly from the $R(\theta, d)$ fits. Despite the low coefficient of determination for the 160 minute data ($r^2 = 0.322$), the consistent increase in the R values indicates a reduction of FeF_2 in the near-surface region.

These ARXPS results show that the progression of the conversion reaction into the $FeF_2(110)$ surface occurs in three distinct phases. At low lithium exposures the reaction front is planar, and hence the reacted region forms

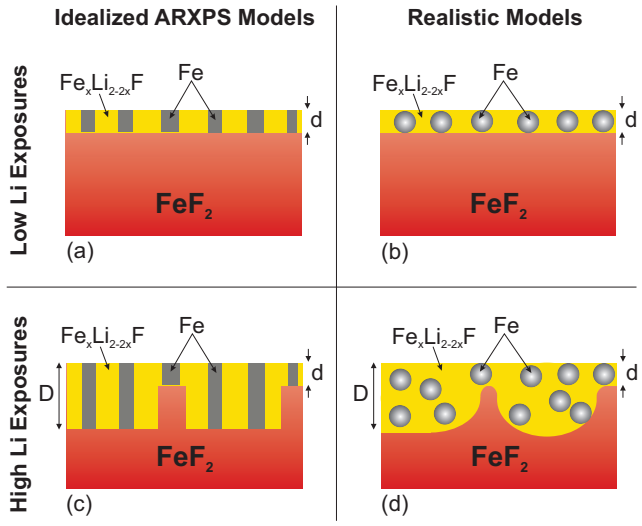

FIG. 6: Idealized models used to simulate ARXPS peak intensiy ratios for the Fe^0 + $Fe_xLi_{2-2x}F_2$ overlayer produced when an $FeF_2(110)$ surface reacts with atomic lithium for overlayer thicknesses (a) < 2 nm and (c) > 2 nm. Corresponding realistic models, based on TEM and MRI data,[5,9,10] for overlayers of thickness (b) < 2 nm and (d) > 2 nm.

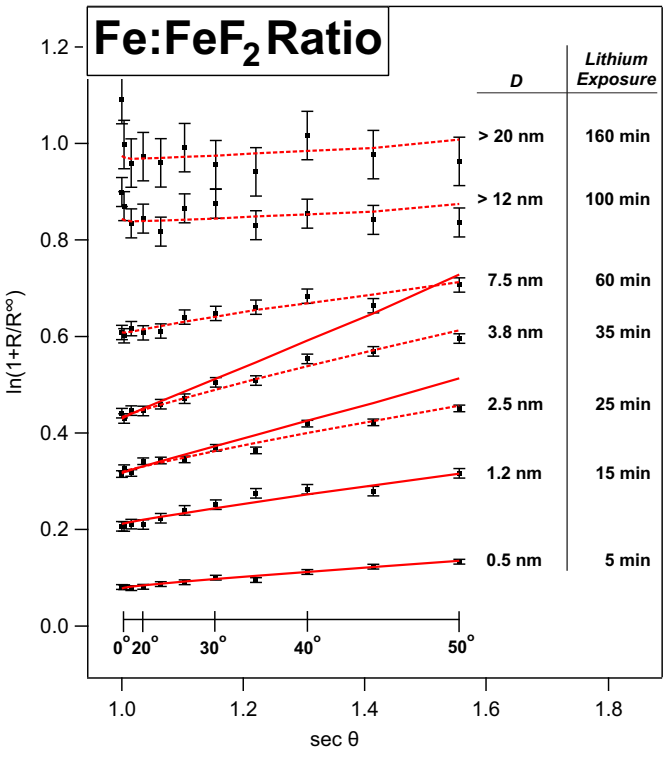

FIG. 7: Linearized $R(\theta, d)$ plots for several different Li exposures. Solid red lines correspond to fits assuming a uniformly thick reacted overlayer (cf., Figs. 6(a) and 6(b)), while dashed lines correspond to fits assuming overlayers with non-uniform thickness (cf., Figs. 6(c) and 6(d)). The quality of each fit is given in Table I.

a uniformly thick overlayer on the $FeF_2(110)$ substrate.

Li Exposure	d (nm)	D (nm)	% Thin Layer	r^2
5 min	0.5 ± 0.1	0.5 ± 0.1	$< 2\%$	0.958
15 min	1.2 ± 0.1	1.2 ± 0.1	$< 5\%$	0.938
25 min	1.2 ± 0.2	2.5 ± 0.3	$13 \pm 2\%$	0.955
35 min	1.2 ± 0.2	3.8 ± 0.3	$13 \pm 2\%$	0.978
40 min	1.2 ± 0.2	4.8 ± 0.4	$13 \pm 2\%$	0.938
45 min	1.2 ± 0.2	5.5 ± 0.5	$12 \pm 2\%$	0.979
60 min	1.2 ± 0.2	7.5 ± 0.7	$13 \pm 2\%$	0.907
100 min	1.2 ± 0.2	> 12	$10 \pm 1\%$	0.800
160 min	1.2 ± 0.2	> 20	$8 \pm 1\%$	0.322

TABLE I: Summary of the reaction front depth and homogeneity for several different Li exposures, where d is the thickness of the homogeneous surface layer, D is the total penetration depth of the conversion reaction, and % Thin Layer is the percentage of the surface occupied by the thinner reacted overlayer and is a measure of the amount of unreacted FeF_2 remaining in the near-surface region. The quality of the fit for each lithiation step is given by r^2.

This is consistent with MD simulations,[11] and can be understood intuitively since the [110] channels into the $FeF_2(110)$ film have a high kinetic barrier for Li transport which prevent lithium diffusion directly into the bulk of the film. Consequently, reaction front remains planar until the reacted overlayer reaches a thickness of ~ 1.2 nm. Upon further lithium exposures, the reacted overlayer thickness becomes non-uniform and can be modeled by a thick (> 2.5 nm) $Fe^0/Fe_{0.5}LiF_2$ overlayer occupying $\sim 87\%$ of the FeF_2 surface, while the remainder of the overlayer remains ~ 1.2 nm thick. This can also be interpreted as 13% of the near-surface FeF_2 remaining unreacted. One possible mechanism causing this non-planar reaction front is preferential Li diffusion along the $Fe^0/Fe_{0.5}LiF_2$ interfaces, resulting in localized regions in which Li is able to reach the underlying FeF_2 and react. Lastly, when the reacted overlayer becomes thicker than ~ 7.5 nm, the percentage of unreacted FeF_2 is observed to decrease from 13% to 8% upon further lithium exposures. The persistence of these unreacted FeF_2 regions suggest that the FeF_2 becomes trapped within the $Fe_{0.5}LiF_2$ matrix. This loss of active cathode material could partially explain the capacity losses observed in cycled FeF_2 cells.

IV. CONCLUSION

Epitaxial $FeF_2(110)$ thin films were exposed to atomic Li in an ultra-high vacuum environment as a solid state analogue for the discharge of FeF_2 conversion batteries. Chemical state analysis using XPS showed the presence of an iron compound identified as $Fe_{0.5}LiF_2$, which agrees with pair distribution function and XPS measurements of electrochemically cycled FeF_2 electrodes.[4,6] ARXPS of the lithiated FeF_2 showed that the reaction initially proceeded in a layer-by-layer manner. This is attributed to the low diffusivity of lithium into FeF_2 [110] channels. When the reacted region became thicker than 1.2 nm,

grain boundaries between the metallic Fe^0 and $Fe_{0.5}LiF_2$ facilitated preferential Li diffusion into the film, leading to a non-planar reaction front and hence regions of unreacted FeF_2, in agreement with MD simulations.[11]

This work shows that the $FeF_2(110)$ crystalline face is reactive with Li despite the high kinetic barrier for Li diffusion directly into the crystal. However, the incomplete reduction of FeF_2 in the near surface regions suggests that FeF_2 might become trapped in the $Fe_{0.5}LiF_2$ matrix that forms upon lithiation. This could lead to a loss of active conversion material and hence a loss in capacity upon cycling as seen in FeF_2 conversion materials. Additionally, the formation of $Fe_{0.5}LiF_2$ prevents iron ions in the cathode from being fully reduced upon lithium exposure, further diminishing the charge storage capacity of FeF_2 electrodes.

In order to gain more insight into the reactivity of FeF_2, additional ARXPS studies will be performed on the $FeF_2(001)$ surface. A thorough characterization of the $Fe_{0.5}LiF_2$ compound with TEM to determine its structure and location in lithiated FeF_2 will be crucial in developing a complete understanding of the Li-FeF_2 reaction. Additionally, a comprehensive study of the effect of Li exposure rate would shed light on the nature of the kinetic limitations of the Li-FeF_2 reactions. Lastly, the use of thin FeF_2 films on conducting substrates could also allow for scanning tunneling microscopy imaging of the FeF_2 surface after small Li exposures. This would further elucidate the mechanism by which Li reacts with both the (110) and (001) surfaces.

Associated Content

More information about the identification of the $Fe_{0.5}LiF_2$ XPS component and the model used to generate $R(\theta, d)$ curves is reported in the Supporting Information. XPS spectra from electrochemically cycled FeF_2 cathodes and from lithiated iron oxide powders are also presented.

Acknowledgements

This work was supported by the Northeastern Center for Chemical Energy Storage, an Energy Frontier Research Center funded by the U.S. DOE, BES under award No. DE-SC0001294. This work also involved the use of instrumentation supported by NSF grant numbers DMR-1126468, which funded the Helium Ion Microscope and DMR-0923246, which funded the XPS system. R.T. was supported by National Science Foundation Grant No. 0903661: Nanotechnology for Clean Energy IGERT. Samples were fabricated and initially characterized at UCSD. The research at UCSD was supported by the Office of Basic Energy Science, U.S. Department of Energy, BES-DMS funded by the Department of Energys Office of Basic Energy Science, DMR under Grant No. DE FG02 87ER-45332. The authors would also like to thank Prof. Torgny Gustafsson for the HIM measurements and Prof. Stephen Garofalini for fruitful discussions.

* Fellow, Nanotechnology for Clean Energy IGERT
† Electronic address: bart@physics.rutgers.edu
‡ Current address: Institut Laue-Langevin, 71 avenue des Martyrs, 38000 Grenoble, France

[1] F. Badway, F. Cosandey, N. Pereira, and G. G. Amatucci, Journal of the Electrochemical Society **150**, A1318 (2003).
[2] F. Badway, N. Pereira, F. Cosandey, and G. G. Amatucci, Journal of the Electrochemical Society **150**, A1209 (2003).
[3] G. Amatucci and N. Pereira, Journal of Fluorine Chemistry **128**, 243 (2007).
[4] J. Ko, K. Wiaderek, N. Pereira, T. Kinnibrugh, J. Kim, P. Chupas, K. Chapman, and G. Amatucci, Appl. Mat. Interfaces **6**, 10858 (2014).
[5] S. Rangan, R. Thorpe, R. A. Bartynski, M. Sina, F. Cosandey, O. Celik, and D. D. T. Mastrigiovanni, The Journal of Physical Chemistry C **116**, 10498 (2012).
[6] M. Sina, R. Thorpe, S. Rangan, R. Bartynski, G. Amatucci, and F. Consandey, In preparation (2014).
[7] H. Li, P. Balaya, and J. Maier, Journal of The Electrochemical Society **151**, A1878 (2004).
[8] M. S. Whittingham, Chem. Rev. **104**, 4271 (2004).
[9] F. Wang, R. Robert, N. Chernova, N. Pereira, F. Omenya, F. Badway, X. Hua, M. Ruotolo, R. Zhang, L. Wu, et al., J. Am. Chem. Soc. **133**, 18828 (2011).
[10] F. Wang, H.-C. Yu, L. Wu, N. Pereira, K. Thornton, A. V. der Ven, Y. Zhu, G. Amatucci, and J. Graetz, Nat. Comm. **3**, 1 (2012).
[11] Y. Ma and S. Garofalini, J. Am. Chem. Soc. **134**, 8205 (2012).
[12] Y. Ma and S. Garofalini, Phys. Chem. Chem. Phys. **16**, 11690 (2014).
[13] T. L. Barr and S. Seal, J. Vac. Sci. Tech. **13**, 1239 (1995).
[14] S. Kowalczyk, L. Ley, F. McFeely, and D. Shirley, Physical Review B **11**, 1721 (1975).
[15] J. F. Watts and J. Wolstenholme, *An Introduction to Surface Analysis by XPS and AES* (2003).
[16] A. Jablonski and C. Powell, Surf. Sci. Rep. **47** (2002).
[17] A. Jablonski and C. Powell, Surf. Sci. **520** (2002).
[18] C. Powell and A. Jablonski, Nucl. Instr. Meth. Phys. Res. **A601** (2009).

[19] C. Powell and A. Jablonski, *NIST Electron Effective-Attenuation-Lenth Database, Version 1.3, SRD 82* (National Institute of Standards and Technology, Gaithersburg, MD, 2011).
[20] A. Nelson, J. Appl. Cryst. **39**, 273 (2006).
[21] A. Grosvenor, B. Kobe, M. Biesinger, and N. McIntyre, Surf. Interface Anal. **36**, 1564 (2004).
[22] T. Fujii, F. de Groot, G. Sawatzky, F. Voogt, T. Hibma, and K. Okada, Phys. Rev. B **59**, 3195 (1999).
[23] S. Kerber, J. Bruckner, K. Wozniak, S. Seal, S. Hardcastle, and T. Barr, J. Vac. Sci. Technol. A **14**, 1314 (1996).
[24] S. Yamamoto, H. Bluhm, K. Anderson, G. Ketteler, H. Ogasawara, M. Salmeron, and A. Nilsson, J. Phys. Condens. Matter **20** (2008).
[25] P. C. Graat and M. A. Somers, Applied Surface Science **100**, 36 (1996).
[26] M. Kasrai and D. Urch, J. Chem. Soc., Faraday Trans. 2 **75**, 1522 (1979).